Molecular Crystals and Liquid Crystals
Publication details, including instructions for authors and subscription information:
http://www.tandfonline.com/loi/gmcl20

Evaluation of TiO_2 Nanotubes Changes after Ultrasonication Treatment

Claudiu Constantin Manole [a], Cristian Pirvu [a] & Ioana Demetrescu [a]
[a] Faculty of Applied Chemistry and Materials Science, University Politehnica Bucharest, Bucharest, Romania

Version of record first published: 28 May 2010

To cite this article: Claudiu Constantin Manole, Cristian Pirvu & Ioana Demetrescu (2010): Evaluation of TiO_2 Nanotubes Changes after Ultrasonication Treatment, Molecular Crystals and Liquid Crystals, 521:1, 84-92

To link to this article: http://dx.doi.org/10.1080/15421401003715850

Mol. Cryst. Liq. Cryst., Vol. 521: pp. 84–92, 2010

ISSN: 1542-1406 print/1563-5287 online
DOI: 10.1080/15421401003715850

Taylor & Francis
Taylor & Francis Group

Evaluation of TiO_2 Nanotubes Changes after Ultrasonication Treatment

CLAUDIU CONSTANTIN MANOLE,
CRISTIAN PIRVU, AND IOANA DEMETRESCU

Faculty of Applied Chemistry and Materials Science,
University Politehnica Bucharest, Bucharest, Romania

A study was undertaken on the influence of ultrasonication over the second-generation TiO_2 nanotubes structured matrix. A 60 V applied voltage for 2 hours anodizing was used to create the ordered structures, with a high voltage power source in low water glycerol electrolyte. The results were investigated using Environmental Scanning Electron. The ultrasonication was performed after anodizing using an ultrasonic cleaner. In correlation to different ultrasonication times, a variance of nanotubes/nanopores was observed. The atomic composition at the surface indicates proportionality between Ti and O in the nanostructures layers and an increase in fluorine with the increase of ultrasonication time. These measurements give information on the wall composition as nanotubes layers are removed through the ultrasonication process. The surface analysis and roughness evaluation of the Ti/TiO_2 nanotube surface were completed with Atomic Force Microscopy (AFM) using an atomic force microscope. The electrochemical behavior of the nanotubes structured surface was performed using electrochemical impedance spectroscopy (EIS).

Keywords AFM characterization; EIS; nanotubes; TiO_2

Introduction

With the success of the TiO_2 nanotubes growth by Zigwilling and his coworkers [1] in 1999 a path was opened for the wide interest over these highly ordered nanostructures. This interest was due to the simple process of growth through anodizing. A variance of conditions related to the voltage, pH electrolyte compositions and time of electrolysis [2,3] lead to nanotubes with various properties and conformations regarding the diameters, lengths and heights [4–7]. These nanostructures present different optimum configurations for a wide appliance field, suited for biocompatibility area [8,9], gas sensing [10–12], self-cleaning [13,14], solar energy conversion [15], hydrogen generation [16,17], wettability [18], photocatalysis [19]. Due to the exposure to ultrasonic treatment in water bath over a prolonged period of time, some changes in surface morphology and topography can be observed. These changes are

Address correspondence to Claudiu Constantin Manole, Faculty of Applied Chemistry and Materials Science, University Politehnica Bucharest, Str. Polizu 1-7, sector 6, Bucharest 011061, Romania. Tel.: +4021.402.39.30; Fax: +4021.311.17.96; E-mail: claudiu.manole@ymail.com

underlined by the electrochemical measurements that have indicated different properties regarding the action of the ultrasonication over the surface. The ultrasonication is described as an intense and violent phenomenon of surface modifications due to the action of a ultrasonic bubble that releases intense energy at its collapse in the liquid environment, over the solid surface. The extended time period of the exposure to ultrasonication resulted in a statistical modification of the surface, generating two different surface structures of the same nanoarchitectures. Thus, a nanopore towards nanotube aspect over the surface was attained. These two different configurations present new perspectives related mainly to the different TiO_2 geometries at the surface, resulting in the overall change of the nanostructures properties.

Experimental

For the experiments titanium electrodes of 99.6% purity from Goodfellow Cambridge Ltd. UK where used. Before the electrochemical process, the titanium disks where manually polished with silicon-carbide paper of increasing granularity of 600, 1000, 1200, 2400 and 4000 until a mirror-like surface was achieved, a final rinse with distilled water being applied. All the electrochemical data were recorded at room temperature using a conventional three electrodes cell: a working electrode, a platinum counter-electrode and an Ag/AgCl, KCl reference electrode connected to Autolab PGSTAT 302 N potentiostat with general-purpose electrochemical system software.

The electrolyte solution used for anodizing was glycerol containing 4% H_2O and 0.36 M NH_4F prepared with ultrapure water. The creation of nanotubes was attained through an anodizing process at an applied voltage of 60 V, using a high-voltage MATRIX MPS-7163 power source. After the electro-oxidation process the samples where rinsed and incubated in a Caloris EG-50 oven at 80°C for 2 hours. Further, the ultrasonication (US) process was achieved using Raypa UCI-150 ultrasonic cleaner. The electrochemical measurements where made at the room temperature using the Autolab PGStat 100. The surface microscopy images were obtained using Environmental Scanning Electron Microscope XL 30 ESEM TMP and Atomic Force Microscope (AFM) from APE Research.

Results and Discussion

Ultrasonication phenomenon overview. The nanostructures were grown through anodizing in glycerol electrolyte with low water content (4% H_2O) and 0.36 M NH_4F as the promoter for the nanostructures formation mechanism. A further US treatment over the obtained samples was applied in order to follow up the changes over its properties and structures over a prolonged period of time for a wide view over the effects on its properties.

The ultrasound energy caused by the sound frequencies in the range of 20 kHz to 50 MHz is the promoter of violent and short lifetime phenomenon. At certain threshold energies [20], cavities are formed due to the collapse of vapor bubbles generating local jets with speeds of 100 m/sec [21] or more and pressure gradients around 1000 atm with hot spot temperatures of about 5000°C and cooling rates above

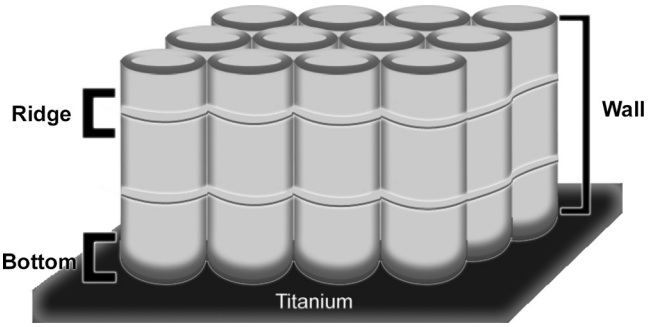

Figure 1. Schematic overview over the nanotubes with its connecting ridges, amorphous wall and semi-crystalline bottom.

10^{10} K/s [23]. These conditions cause a series of changes, generating nanocrystals [24] or enhancing crystallization [25,26] and generating corrosion [27], leading to modifications of the properties' exposed surface. The formation of these cavities on the TiO_2 surface can be observed preponderant in Figure 2e) and f) after the 30 min and 35 min of US time. The time period used for this experiments is much too extended in order to surprise immediate short-lived effects, but large enough to follow the significant changes in the conformation of these nanostructures.

Concerning the atomic structure, it has been reported that the nanotubes have an amorphous tube wall and semi-crystalline barrier layer at the bottom [28]. The wall presents horizontal ridges that connect individual nanotubes (Fig. 1). These ridges, characteristic to nanotubes grown in aqueous, ethylene glycol [29] and glycerol electrolytes [30] give an increased mechanical resistance over horizontal planes. These three elements – amorphous tube walls, barrier oxide layer at the bottom and ridge connection of individual nanotubes – can be the key factors in creating layered areas exposed in the US process and results in a different morphological and topographical distribution of the nanostructures.

SEM evaluations. After the US process a variance from nanopores (as seen in Fig. 2a) towards nanotubes aspect can be observed. Random slits formed by the combination of two or more nanopores are highlighted. These slits can be the center for further cavitations in the US process. The specific cavitation can be marked out especially in Figure 2e) for the 30 min US. After 25 minutes and 35 minutes of US process a tubular-like shape nanostructures emerge (Fig. 2d and 2f). The diameter for the 20 minutes US nanotubes (Fig. 2c) walls varies between 25 nm and 35 nm and for the 15 minutes US time (Fig. 2b) between 37 nm and 57 nm.

In the case of multilayered removal of the grown TiO_2 oxide, this clear change in the morphology of the nanotubes can offer a glimpse into the thinning of the walls due to the process of fluoride attack over the current resistive oxide.

Over US time, an overall interior volume of the nanostructures constraint can be observed, as the internal diameter shortens.

The SEM EDS measurements revealed that besides titanium and oxygen, in the grown nanostructures fluorine is also present.

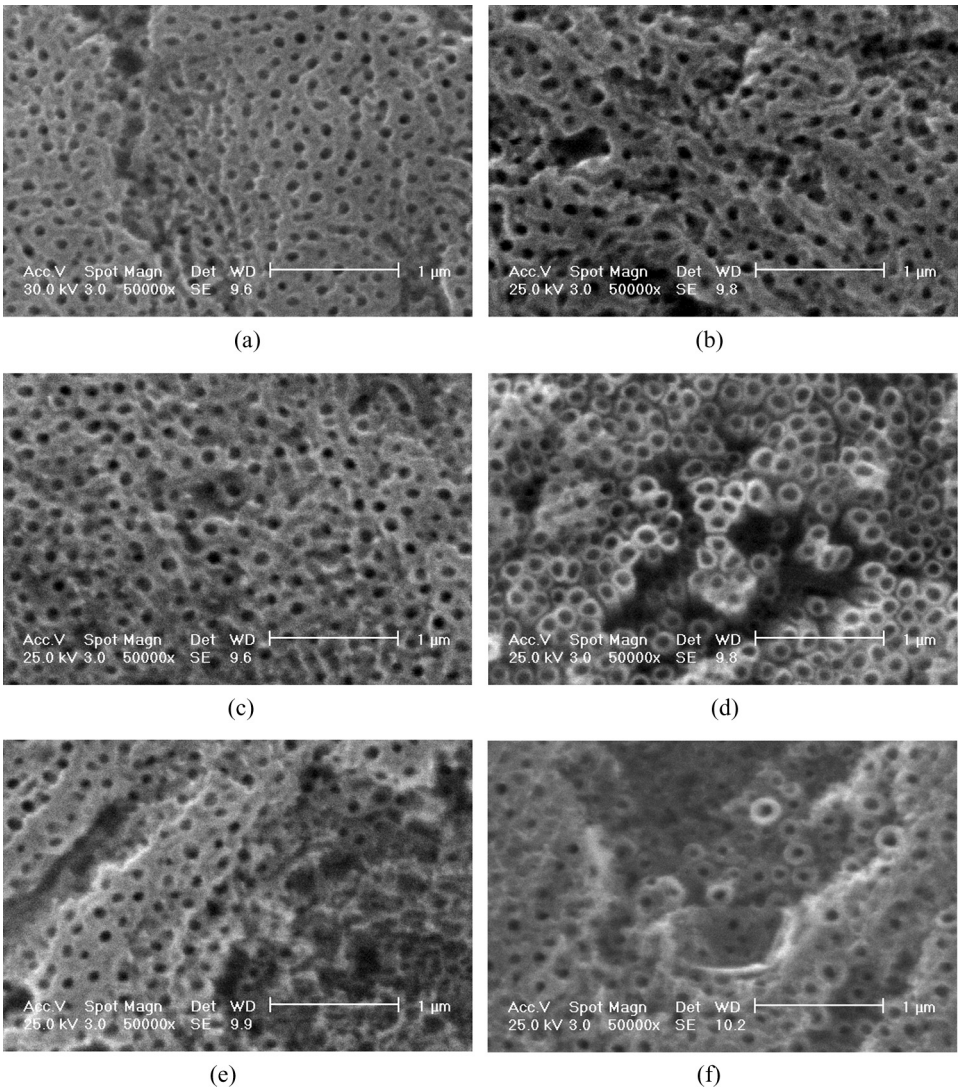

Figure 2. Nanostructures morphology after the US times: (a) 0 min, (b) 15 min, (c) 20 min, (d) 25 min, (e) 30 min, (f) 35 min; the cavity formed by the ultrasonic bubble can be observed for the last three US times.

Treated at different US times, as it was expected, after layer by layer exposure under the intense and short lived US effects, the surface atomic proportion suffers modifications (Fig. 3).

After this layered exposure, due to the presented morphological components, as highlighted in the US phenomenon overview, in the sample that was not subjected to US treatment an important percentage of fluorine (8.95%) is presented in the structures.

After 15 minutes of US, the percentage of fluorine decreases drastically to 7.59%, followed by a stable increase to 9.83% for the 30 min US time. This is an

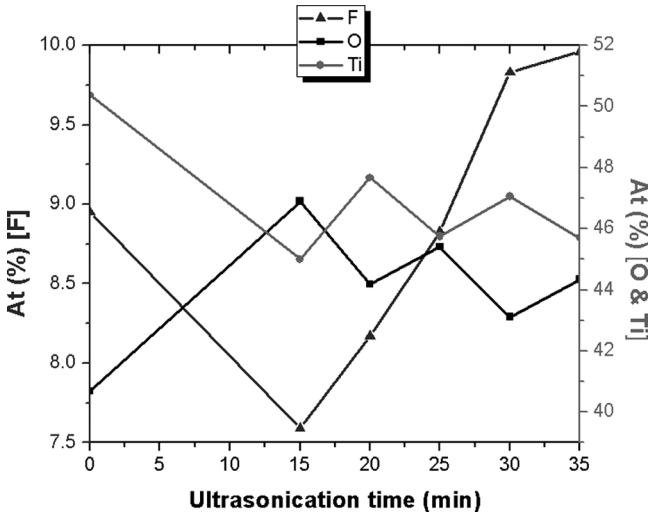

Figure 3. Atomic proportions for the SEM 5 μm^2 scanned areas; a strong variation in fluor is observed.

indication that points out the retention of fluorine as a consequence of the formation mechanism of the nanostructures. At the final 35 min US time the percentage value reaches the highest point of 9.96%. This suggests that, during the extended US times of determining the specific structural changes, the changes defined by the stages of nanostructures growth [31] present a fluoride retention that is incorporated in the TiO_2 nanostructure.

AFM results. The data were processed, applying leveling by mean plane subtraction and proceeding with corrections over the horizontal strokes. The normalized histograms of the heights for the AFM images at different US times (Fig. 4) provided the following statistical data.

Due to the planarity of the 0 min US surface shown in SEM image (Fig. 2a), the AFM cantilever tip of 10 μm encounters topography with small heights, the typical height of around 0.05 μm being detected. At 15 min US (Fig. 4b) the investigated surface presents higher frequencies for the heights around 0.2 μm. The measured area at 30 min US and 35 min US (Fig. 4e and f) present a statistical distribution of the maximum heights at 0.26 μm and 0.11 μm respectively. For 20 min US and 25 min US (Fig. 4c and d) the widest plane of high densities for heights with an interval of 50 nm each is obtained.

Samples with no US applied, and the last one of 35 min US, present maximum heights of about 135 nm (±35 nm). As for the rest of the US samples the average maximum height is calculated at 334 nm (±36 nm).

Electrochemical results. The electrochemical measurements were made in a simulated body fluid (SBF). The serum used was a variation of the Hank solution with 8 g/L NaCl, 0,4 g/L KCl, 0.35 g/L $NaHCO_3$, 0.25 g/L $NaH_2PO_4 \cdot H_2O$, 0.06 g/L $Na_2HPO_4 \cdot 2H_2O$, 0.19 g/L $CaCl_2 \cdot 2H_2O$, 0.19 g/L $MgCl_2$, 0.06 g/L $MgSO_4 \cdot 7H_2O$, 1 g/L glucose. The data processing from the Autolab PG-Stat 100 measurements were made using Nova 1.4 software. Reference EIS

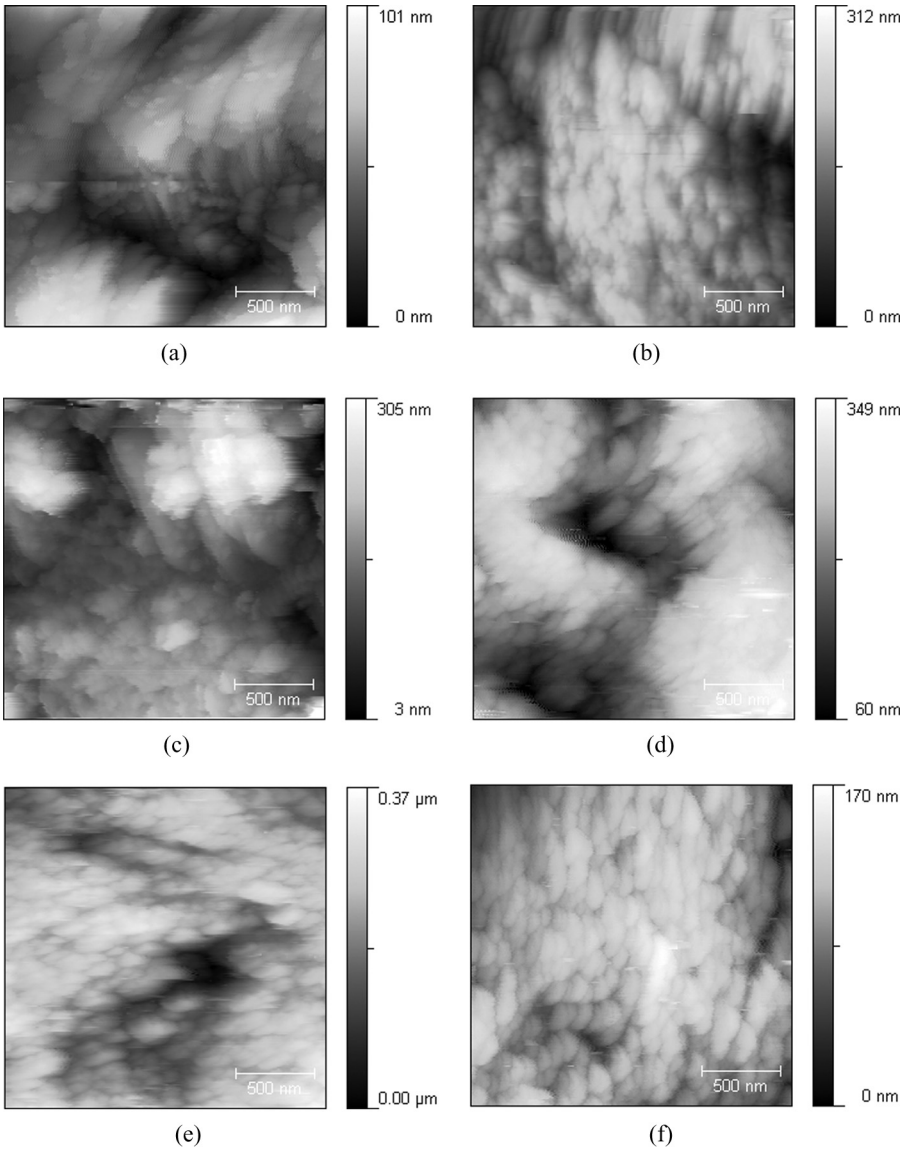

Figure 4. AFM image and its corresponding height distribution to the right, where (a) is for 0 min US, (b) 15 min US, (c) 20 min US, (d) 25 min US, (e) 30 min US and (f) 35 min US. The highlighted area for 0 min US indicates a bimodal mixture of two normals, with contributions to the rest of the US samples.

measurements were made using an untreated Ti sample. The initial fitting of the EIS circuit measured in the SBF was made starting from the assumption of one circuit defined by the charge resistance R_{ct} and a constant phase circuit value (CPE) Q_{ct}. The fitting result is shown in Figure 5.

Due to the high US times with respect to the short-lived violent effects of the implicated phenomenon, the general study on certain large time intervals presents an overall evaluation of the statistical events over the treated surfaces.

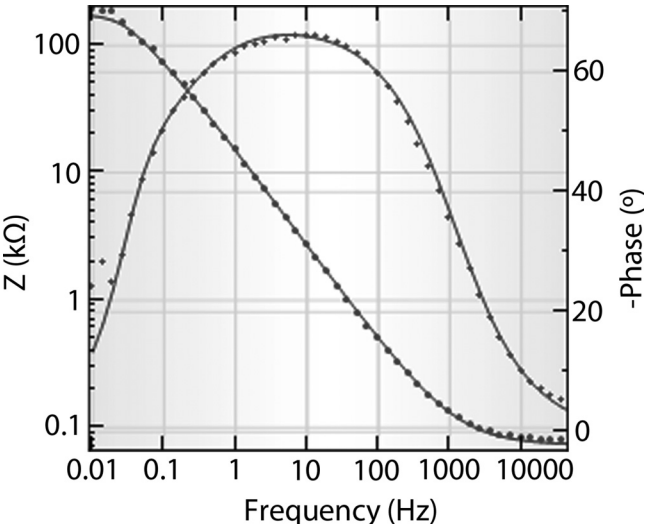

Figure 5. Electrochemical measurement Bode fits for titanium.

The circuit fitting for the EIS is made having three modules connected in series and is represented in Figure 6.

Table 1 expresses the values as circuit results, data that present different behaviors for the samples with no US and the final 35 min US sample.

The nanostructures' experimental fitting results indicate a decrease of the resistance, as the final conformation of the nanostructures takes place after the statistical effect of the US bubble over the long period of time. For both samples the behavior is preponderant capacitive, with a slight tendency towards diffusion for the 35 min US sample. The pseudocapacitance of the constant phase element presents a clear decrease as it drops with around 60% at the fitted US sample.

Regarding to the charge transfer, the pseudocapacitance has a drop of about 27% from the sample with no US towards the 35 min US sample. The n_{ct} factor indicates a tendency towards diffusion for the TiO_2 with no US treatment applied, and a strong resistive value for the sample at 35 min of US. These results can be related to

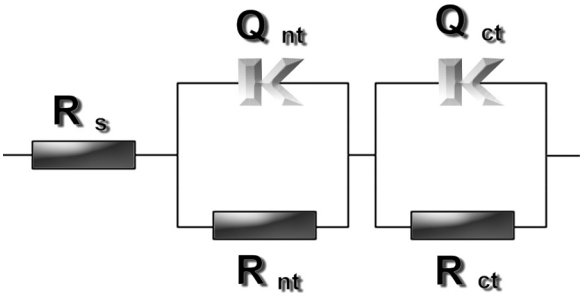

Figure 6. The used circuit for the EIS data fit; Notations: R_s – solution resistance; R_{nt}, Q_{nt} – the resistance and the CPE for the nanotubes; R_{ct}, Q_{ct} – the resistance and the CPE for the charge transfer.

Table 1. Simulated values for the EIS fit circuit; R_s – solution resistance; R_{nt} the resistance for the nanotubes; R_{ct} the resistance for the charge transfer, CPE_{nt} and CPE_{ct} are the constant phase elements for nanotubes and charge transfer respectively, n_{nt} – n_{ct} is the depression angle for nanostructures – charge transfer respectively indicating the capacitive/resistive behavior

Sample	R_s (Ω)	R_{nt} (MΩ)	CPE_{nt}	n_{nt}	R_{ct} (kΩ)	CPE_{ct}	n_{ct}	Chi square
0 min US	132,00	15,00	110,00	0,76	12,60	81,30	0,65	0,18
35 min US	123,00	5,00	43,60	0,69	16,70	111,00	0,82	0,23

the fluoride remaining at the nanostructures' interface after rinsing and drying and prior to anodizing, which might be activated by the low amplitude EIS potential of ±10 mV at different frequencies.

Conclusions

The ultrasonication effects over the TiO_2 highly ordered nanostructures' surface were investigated. The extreme events taking place at this surface through the action of the ultrasonication effects lead to changes in morphology and implicitly in the topography.

A nanotube/nanopore variance through ultrasonic treatment was achieved.

In regard to the nanostructures' diameter, the SEM images indicate that nanotubes areas are more reproductively than nanopores with respect to the pores area, with 3 and 3.5 μm^2 differences in the diameters. After extended ultrasonication times, a thickening of the tube walls can be observed.

The EIS data corresponds to a circuit where electrochemical parameters are found for the fitted model that takes into consideration the SBF resistance, charge transfer and nanostructures contribution. The EIS results denote an important contribution with respect to the electrochemical properties due to the statistical action of the ultrasonic bubble over the nanoarchitectures.

Acknowledgments

The authors gratefully acknowledge the financial support of the Romanian National CNCSIS Grant IDEI No. 624/2008.

References

[1] Zwilling, V., Darque-Ceretti, E., Boutry-Forveille, A., David, D., Perrin, M. Y., & Ancouturier, M. (1999). *Surf. Interface Anal.*, *27*, 629.
[2] Ghicov, A., Tsuchiya, H., Hahn, R., Macak, J. M., & Munoz, A. G. (2006). *Electrochem. Commun.*, *8*, 528.
[3] Man, I., Pirvu, C., & Demetrescu, I. (2008). *Rev. de Chimie*, *59*, 615.
[4] Mor, G. K., Varghese, O. K., Paulose, M., Shankar, K., & Grimes, C. A. (2006). *Sol. Energy Mater. Sol. Cells*, *90*, 2011.
[5] Macak, J. M., Tsuchiya, H., Taveira, L., Aldabergerova, S., & Schmuki, P. (2005). *Angew. Chem. Int. Ed.*, *44*, 7463.

[6] Albu, S. P., Ghicov, A., Macak, J. M., & Schumuki, P. (2007). *Phys. Status Solidi.*, *1*, R-65–R-67.
[7] Raja, K. S., Misra, M., & Paramguru, K. (2005). *Electrochim. Acta*, *51*, 154.
[8] Karla, S. B., Seunghan, O., Christine, J. C., Lars, M. B., Henri, H., & Sungho, J. (2009). *Acta Biomaterialia*, in press.
[9] Tsuchiya, H., Macak, J. M., Muller, L., Kunze, J., Muller, F., Greil, P., Virtanen, S., & Schmuki, P. (2006). *Wiley Interscience*, *77A*, 534.
[10] Zakrzewska, K., Radecka, M., & Rekas, M. (1997). *Thin Solid Films*, *310*, 161.
[11] Rothschild, A., Edelman, F., Komem, Y., & Cosandey, F. (2000). *Sens. Actuat., B*, *67*, 282.
[12] Seo, M., Yuasa, M., Kida, T., Huh, J., Yamazoe, N., & Shimanoe, K. (2009). *Procedia Chemistry*, *1*, 192.
[13] Fujishima, A., Honda, K., & Kikuchi, S. (1969). *Chem. Soc. Jpn.*, *72*, 282.
[14] Fujishima, A. & Honda, K. (1972). *Nature*, *238*, 37.
[15] Regan, B. O. & Gratzel, M. (1991). *Nature*, *737*, 353.
[16] Liu, Zhaoyue, Pesic, Batric, Raja, Krishnan S., Rangaraju, Raghu R., & Misra, Mano (2009). *Int. J. Hyd. Energy*, *34*, 3250.
[17] Kim, E. Y., Park, J. H., & Han, G. Y. (2008). *J. of Power Sources*, *184*, 284.
[18] Wang, R., Hashimoto, K., Fujishima, A., Chikuni, M., Kojima, E., Kitamura, A., Shimohigoshi, M., & Watanabe, T. (1997). *Nature*, *338*, 388.
[19] Mils, A., Hill, G., Bhopal, S., Parkin, I. P., & O'Neill, S. A. (2003). *J. Photochem. Photobiol. A.*, *160*, 185.
[20] Rozenberg, L. D. (1971). *High-intensity Ultrasonic Fields*, Plenum: New York.
[21] Plesset, M. S., & Chapman, R. B. J. (1971). *Fluid Mech.*, *47*, 283.
[22] Suslick, K. S., Casadonte, D. J., Green, M. L. H., & Thompson, M. E. (1987). *Ultrasonics*, *25*, 56.
[23] Suslick, K. S., & Crum, L. A. (1997). *Encyclopedia of Acoustics*, Crocker, M. J. (Ed.), Chapter 1, Wiley-Interscience: New York, 271–282.
[24] Brown, Suree S., Im, Hee-Jung, Rondinone, Adam J., & Dai, Sheng (2005). *J. Colloid Interface Sci.*, *292*, 127.
[25] Ueno, S., Takeuchi, M., Sakata, J., Nozue, Y., Amemiya, Y., & Sato, K. (2003). *KEK Prog Rep*, *93*, 2002-2.
[26] Jun'Ichi, S., Satoru, U., & Kiotaka, S. (2001). *Nihon Yuka Gakkai Nenkai Koen Yoshishu*, *40*, 115.
[27] Preece, C. M., & Hansson, I. L. (1981). *Adv. Mech. Phys. Surf.*, *1*, 199.
[28] Nguyen, Q. A. S., Bhargava, Y. V., Radmilovic, V. R., & Devine, T. M. (2009). *Electrochimica Acta*, *54*, 4340.
[29] Macak, J. M., Tsuchiya, H., Taveira, L., Aldabergerova, S., & Schmuki, P. (2005). *Angewandte Chemie International Edition*, *44*, 7463.
[30] Valota, A., LeClere, D. J., Skeldon, P., Curioni, M., Hashimoto, T., Berger, S., Kunze, J., Schmuki, P., & Thompson, G. E. (2009). *Electrochimica Acta*, *54*, 4321.
[31] Manole, C. C., Pirvu, C., & Demetrescu, I. (2009). *Key Eng. Mat.*, *415*, 5.